Journal of Catalysis **194,** 153–166 (2000)
doi:10.1006/jcat.2000.2918, available online at http://www.idealibrary.com on IDEAL®

Effect of Titanium Substitution in ≈$SbVO_4$ Used for Propane Ammoxidation

Andreas Wickman,* L. Reine Wallenberg,† and Arne Andersson*,[1]

*Department of Chemical Engineering II; and †Department of Inorganic Chemistry II, Center for Chemistry and Chemical Engineering, Lund University, P.O. Box 124, SE-221 00 Lund, Sweden

Received March 6, 2000; revised April 20, 2000; accepted May 3, 2000

Catalysts of the nominal composition $Sb_{0.9}V_{0.9-x}Ti_xO_y$, $0.0 \leq x \leq 0.9$, were prepared and characterized with X-ray diffraction, Fourier transform-Raman spectra, diffuse reflectance infrared Fourier transform spectra, transmission electron microscopy, electron diffraction, and X-ray microanalysis. The catalysts were used for the ammoxidation of propane to give acrylonitrile. Compared with the pure ≈$SbVO_4$ ($Sb_{0.92}V_{0.92}O_4$) it is observed that the activity decreases while the selectivity to acrylonitrile formation is improved when the Ti : V ratio of the preparation is increased. The characterization of the catalysts shows the formation of a rutile-type phase in all preparations with vanadium. Additionally, α-Sb_2O_4 is formed in an amount that increases with the amount of titanium in the sample. X-ray microanalysis data confirm that two substitution mechanisms occur in parallel, namely, one Ti^{4+} substitutes for one V^{4+} and two Ti^{4+} substitute for one V^{3+} and one Sb^{5+}, forming the solid solution series $Sb^{5+}_{(0.92-z/2)}V^{3+}_{(0.28-z/2)}V^{4+}_{(0.64-u)}Ti^{4+}_{(z+u)}\square_{0.16}O_4$ (□ is a cation vacancy). Quantitative model calculations considering data obtained by the characterization methods give the content of cations in the unit cell of the rutile phase. It is demonstrated that the activity can be correlated with the content of V^{3+} in the unit cell, indicating that the activation of propane occurs on a V^{3+} center. Moreover, the selectivity to acrylonitrile can be correlated to the Sb^{5+}/V^{3+} ratio, which indicates that the ammonia is activated on a Sb^{5+} moiety. Considering both activity and selectivity, the best performance for propane ammoxidation is obtained for a sample with the nominal composition $Sb_{0.9}V_{0.3}Ti_{0.6}O_y$. The selectivity to acrylonitrile is 53% at 25% propane conversion to be compared with 12% at 15% propane conversion for the nonsubstituted ≈$SbVO_4$. The improved selectivity can be explained by isolation of the vanadium centers in the active phase, which gives fewer bridging V–O–V moieties that are active for degradation and combustion of propane and the subsequently formed propylene.

Key Words: **propane; ammoxidation; acrylonitrile formation; Sb–V–Ti oxide catalysts; catalyst characterization; XRD; FT-Raman; DRIFT; transmission electron microscopy; electron diffraction; X-ray microanalysis.**

INTRODUCTION

At present, acrylonitrile is produced by the ammoxidation of propylene over either multicomponent bismuth molybdate catalysts or promoted iron antimonates (1, 2). In recent years interest has grown in developing an alternative process using propane instead of propylene as feedstock for acrylonitrile production through direct one-step ammoxidation (1, 2). A main reason for this interest is that propane is considerably more abundant and cheaper than propylene. Moreover, regarding the utilization of natural resources, it is of general interest to develop catalysts for the conversion of natural gas components such as propane to useful products.

A candidate catalyst system for propane ammoxidation is the modified Sb–V–O system (3–5), in which rutile-type ≈$SbVO_4$ is considered to be a crucial catalyst structure (3). Results published in the literature have shown that the pure ≈$SbVO_4$ phase is not active and selective to acrylonitrile formation (6). However, the performance of the catalyst is improved when the Sb : V atomic ratio in the preparation is larger than 1, and the yield to acrylonitrile is further increased by the addition of aluminum and tungsten to the Sb–V–O system (3, 5, 7). A yield to acrylonitrile of almost 40% has been reported for an Al–Sb–V–W oxide catalyst, using feed ratios between propane, oxygen, and ammonia that are stoichiometric regarding the formation of acrylonitrile (5).

Characterization of the Sb–V–O system for propane ammoxidation has revealed that surplus antimony oxide spreads over the surface of an $Sb_{0.92}V_{0.92}O_4$ phase, forming supra-surface antimony sites (8, 9). In the Al–Sb–V–O system the active phase was identified to have the composition $Al_{1-x}SbV_xO_4$ with $0 < x < 0.5$ (7). In addition to being an element of the active phase, the role of aluminum is that of a support. A comprehensive study of the Al–Sb–V–W–O system has shown that the active phase in this system is $Sb_{0.9}V_{0.9-x}W_xO_4$ (5). It should be noticed that ≈$SbVO_4$, (Al,V)SbO_4, and ≈Sb(V,W)O_4 all have the rutile type of structure. (Al,V)SbO_4 can be described as a solid solution between rutile-type $AlSbO_4$ and ≈$SbVO_4$ (7),

[1] To whom correspondence should be addressed. Fax: +46-46-149156. E-mail: Arne.Andersson@chemeng.lth.se.

0021-9517/00 $35.00

and ≈$Sb(V,W)O_4$ is a solid solution between ≈$SbVO_4$ and rutile-type WO_2 (5).

It has been demonstrated that, compared with the pure ≈$SbVO_4$ phase, the better catalytic properties of $(Al,V)SbO_4$ and ≈$Sb(V,W)O_4$ for propane ammoxidation can be rationalized in terms of the site isolation theory. According to this theory, which was originally formulated by Callahan and Grasselli (10), a catalyst being selective for partial oxidation can be developed by creating structural isolation of the active site (11). Thus, the improvement of the selectivity to acrylonitrile formation by substitution of some of the vanadium atoms in ≈$SbVO_4$ with Al or W can be explained by the fact that the substitution creates isolation of the remaining vanadium atoms to a suitable degree, preventing waste formation (5, 7). In Sb_2O_4/≈$SbVO_4$ catalysts supra-surface antimony sites likewise create isolation of active vanadium sites at the surface, giving better catalytic properties than the pure ≈$SbVO_4$ phase regarding propane ammoxidation (12). Also for the ammoxidation of propylene the presence of α-Sb_2O_4 in addition to ≈$SbVO_4$ was observed to be important for the catalytic performance (13, 14).

When prepared from V_2O_5 and Sb_2O_3 by calcination in air the pure ≈$SbVO_4$ phase attains the approximate composition $Sb_{1-x}V_{1-x}O_4$ with $x \approx 0.1$ (15, 16). Moreover, it has been reported that heating of an equimolar mixture of V_2O_5 and Sb_2O_3 under anaerobic conditions produces phases with the compositions $Sb_{1-y}V_{1+y}O_4$ (15) and $Sb_{1-y}VO_{4-1.5y}$, where $y \approx 0.1$ (16). Heating of the oxide mixture in commercial nitrogen with trace oxygen gave the composition $Sb_{1-y}VO_{4-2y}$, where $y \approx 0.1$ (16). Analytical data (15) indicate the composition to be $Sb_{0.92}V_{0.92}O_4$ for the sample being calcined in air. The same composition was found in a more recent investigation (17) in which it was shown that the rutile-type phase is cation deficient, i.e., $Sb^{5+}_{0.92}V^{3+}_{0.28}V^{4+}_{0.64}\square_{0.16}O_4$, where $\square$ denotes cation vacancies. In a comprehensive study (18) it was observed that heating equimolar mixtures of V_2O_5 and Sb_2O_3 at 800°C under flowing gas with varying $O_2:N_2$ ratios produces a continuous nonstoichiometric series of rutile type, i.e., $Sb_{0.9}V_{0.9+x}\square_{0.2-x}O_4$ with $0 < x < 0.2$ and varying amounts of α-Sb_2O_4. It was, moreover, demonstrated that the previously reported compositions (15, 16) all belong to this series.

In light of the site isolation concept and the previous results, it would be of interest to try substitution of some of the vanadium in ≈$SbVO_4$ with titanium. The possibility for titanium substitution is good, since rutile-type TiO_2 exists (19) and the crystal radii of Ti^{4+} (0.61 Å), V^{4+} (0.58 Å), V^{3+} (0.64 Å), and Sb^{5+} (0.60 Å) are of similar size (20). Therefore, one objective of the present study of the Sb–V–Ti–O system was to substitute titanium into the ≈$SbVO_4$ structure to replace vanadium, thus achieving isolation and dispersion of the vanadium sites on the surface of the material. In particular the effect of the degree of isolation and dispersion of the vanadium sites was investigated regarding activity and selectivity. Considering that ≈$SbVO_4$ has both V^{3+} and V^{4+} sites in the bulk of the material and the $Al_{1-x}SbV_xO_4$ phase with only V^{3+} is more selective to acrylonitrile formation (7), another objective of the present investigation was to unravel the substitution mechanism for titanium in ≈$SbVO_4$. Thereby, correlation with activity data can provide more information about the importance of the different valence states of vanadium for propane activation and acrylonitrile formation.

EXPERIMENTAL

Catalyst Preparation

The Sb–V–Ti–O catalysts were prepared from powders of V_2O_5 (Riedel-de Haën, 99.5%), Sb_2O_3 (Merck, ≥ 99%), and TiO_2 (Kebo, ≥ 99%). Pure ≈$SbVO_4$ was prepared by adding 15.4 g of V_2O_5 powder to a mixture of 515 ml of water and 80 g of a 30 wt% hydrogen peroxide solution in water, thus forming peroxovandium ions (21). After 20 min of stirring, 24.6 g of Sb_2O_3 powder was added. The mixture obtained was stirred under cover for 3 h while being heated. Thereafter, in order to reduce the water volume through evaporation the mixture was stirred in the uncovered beaker. When the mixture could no longer be stirred it was dried in an oven at 120°C for 16 h. The dried mixture was then calcined for 16 h at 650°C, cooled, crushed, and sieved to give particles with diameters in the range 150–425 μm. The catalyst was finally calcined in air at 810°C for the duration of 1 h.

A series of catalysts with Ti replacing vanadium, and with the nominal composition $Sb_{0.9}V_{0.9-x}Ti_xO_y$, was prepared with x varying from 0.1 to 0.9 in steps of 0.1 and with y being determined by the valences of the cations. The catalysts were prepared using the same procedure as was used to prepare the ≈$SbVO_4$ catalyst and is described above. The appropriate amount of TiO_2 powder was added immediately before the step involving heating in an uncovered beaker to reduce the water volume.

All the samples prepared were subjected to an intermittent calcination in air at 650°C before the final calcination in air for 1 h at 810°C. The intermittent calcination was performed stepwise with X-ray analysis of the sample in between in order to control the synthesis. The total duration of the intermittent calcination varied between 16 and 24 h depending on the titanium content of the sample. The prepared catalysts with the nominal composition $Sb_{0.9}V_{0.9-x}Ti_xO_y$ are denoted SVT-XYZ, where $X:Y:Z$ is the nominal Sb : V : Ti atomic ratio of the preparation (cf. Table 1).

Activity Measurements

The activity measurements were performed in a conventional laboratory apparatus consisting of a plug-flow reactor

made from quartz glass, working at atmospheric pressure. In order to have isothermal conditions in the reactor the catalysts were diluted with quartz. The reactor temperature was held at 480°C. The ratio of reactants in the inlet flow corresponded to the stoichiometric ratio of propane, ammonia, and oxygen for acrylonitrile formation. In addition to the reactants and nitrogen, water vapor was added to the feed to help to control the temperature of the exothermic reaction (propane : ammonia : oxygen : steam : nitrogen = 1 : 1 : 2 : 0.5 : 2.5). The total inlet flow of 70 ml STP/min was passed over 100–8400 mg of catalyst.

The analysis of propane, propylene, acrylonitrile, acetonitrile, and uncondensable gases was performed on-line with a gas chromatograph equipped with a Porapak Q column, an FID detector, and a methanation column, making possible the analysis of carbon oxides in the form of methane. Ammonia and hydrogen cyanide were analyzed by absorption and titration methods (22).

Characterization of Catalysts

Specific surface areas were measured with a Micromeritics Flowsorb 2300 instrument using the BET method with adsorption of nitrogen at the liquid nitrogen temperature. The catalyst samples were degassed at 350°C. The specific surface areas of the catalysts are given in Table 1.

Diffuse reflectance infrared Fourier transform (DRIFT) spectra were recorded using a Mattson Polaris spectrometer equipped with a liquid nitrogen-cooled broad band MCT detector and a Harrick Scientific Praying Mantis diffuse reflection attachment. The samples were diluted with KBr to give 1 wt% of sample. Spectra were recorded in dry air. A resolution of 4 cm^{-1} was used, and 1000 scans were collected for each sample.

Fourier transform Raman (FT-Raman) spectra were produced using a Bruker IFS 66 FTIR spectrometer equipped with a Bruker FRA 106 FT-Raman device, a Nd : YAG laser, and a germanium diode detector. Measurements were carried out under ambient conditions on uncrushed catalyst particles in 5-mm quartz tubes. The laser power was set at 50 mW, the resolution was 4 cm^{-1}, and 1000 scans were recorded for every spectrum at 180° backscattering.

X-ray diffraction (XRD) patterns were recorded using a Seifert XRD 3000 TT diffractometer with Ni-filtered Cu$K\alpha$ radiation and Si as an internal standard. The measurements were made on ground samples in a rotating sample holder. The unit cell parameters of the rutile-type structure in the catalysts were determined from the eight strongest reflections of the phase.

For transmission electron microscopy (TEM), samples of a representative catalyst (SVT-963) were dispersed in methanol and a drop of the suspension was placed on a copper grid with a holey carbon film. The samples were examined in a Jeol JEM 2000FX transmission electron microscope, equipped with a Link AN 1000 energy dispersive X-ray spectrometer (XEDS). Images and diffractograms were recorded on a Gatan slow-scan CCD camera with a 1028 × 1028 pixel chip. The microscope has a point resolution of 0.27 nm at 200 kV accelerating voltage.

RESULTS

Specific Surface Area

The specific surface areas of the samples are displayed in Table 1 and appear to be uniform and about 3–4 m^2/g for the samples containing both vanadium and titanium. SVT-990 has a lower surface area, which corresponds to the values reported in the literature for the Sb/V system and the ≈$SbVO_4$ tetragonal rutile in particular (7, 12). The substitution of titanium seems to have little effect on the surface area. There is an initial increase in surface area as the first substitution is made, but the surface area does not increase as the amount of titanium present increases. For SVT-909, which contains no vanadium, the surface area is considerably larger.

X-Ray Diffraction

Some typical X-ray patterns of prepared Sb–V–Ti–O catalysts are shown in Fig. 1. The powder diffractogram of the ≈$SbVO_4$ (SVT-990) sample shows only lines from a rutile-type structure. The unit cell parameters for this sample are in Table 2 and show good agreement with the data being reported in the literature for the oxidized ≈$SbVO_4$ (9, 15–17). Lines from a related phase are present in all the samples with titanium up to $x = 0.8$ in nominal $Sb_{0.9}V_{0.9-x}Ti_xO_y$, i.e., for SVT-918. For the latter sample, however, the predominant peaks are from α-Sb_2O_4. Diffraction peaks from α-Sb_2O_4 are clearly visible also in the XRD pattern of SVT-936. For the samples with lower titanium content the lines from α-Sb_2O_4 are weak, and their intensities decrease as the amount of titanium in the sample is decreased (cf. SVT-954 and SVT-972 in Fig. 1). For SVT-981 no reflections

TABLE 1

Notation, Nominal Composition, and Specific Surface Area of Prepared Sb–V–Ti–O Catalysts

Catalyst notation	Atomic ratio Sb : V : Ti	Specific surface area (m^2/g)
SVT-990	9 : 9 : 0	1.67
SVT-981	9 : 8 : 1	3.59
SVT-972	9 : 7 : 2	3.13
SVT-963	9 : 6 : 3	3.80
SVT-954	9 : 5 : 4	3.65
SVT-945	9 : 4 : 5	3.37
SVT-936	9 : 3 : 6	3.29
SVT-927	9 : 2 : 7	3.32
SVT-918	9 : 1 : 8	3.64
SVT-909	9 : 0 : 9	27.32

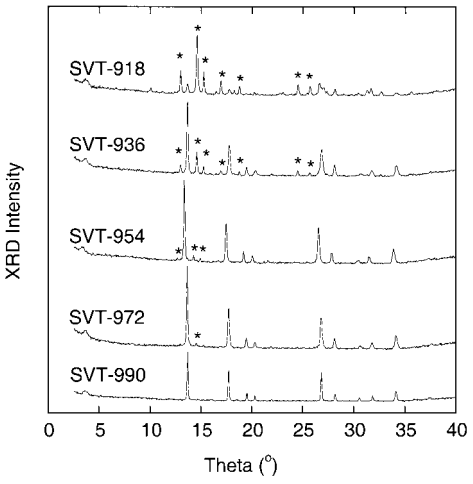

FIG. 1. Representative X-ray diffractograms of Sb–V–Ti–O catalysts showing the presence of a rutile-type phase. Reflections from α-Sb_2O_4 are marked with an asterisk. For clarity the figure shows diffractograms for the samples without Si standard being added and, therefore, the peak positions are not precisely adjusted. Unit cell data obtained using the Si standard are presented in Table 2.

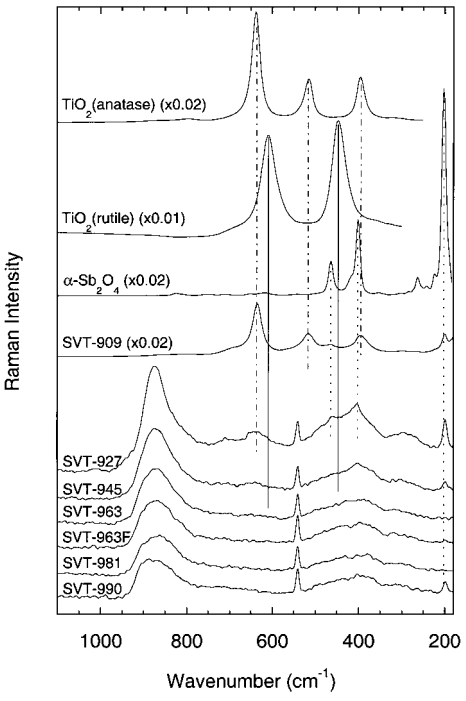

FIG. 2. Raman spectra of some typical Sb–V–Ti–O catalysts after use in propane ammoxidation. For comparative purposes, spectra are shown for freshly prepared SVT-963 (denoted SVT-963F), α-Sb_2O_4, and the rutile and anatase polymorphs of TiO_2. The peak at 540 cm^{-1} is an instrumental artifact peak, which can be used for quantitative comparisons.

from α-Sb_2O_4 were visible. Besides a rutile-type phase and α-Sb_2O_4, the powder diffractograms in Fig. 1 show the presence in the samples of no other phase or phases. Only SVT-909 without vanadium showed the presence of reflections from the anatase polymorph of TiO_2 along with the lines from α-Sb_2O_4.

Unit cell parameters determined for the samples with titanium are collected in Table 2 and compared with those of $\approx SbVO_4$. As is evident from Table 2 there is no significant alteration of the unit cell parameters when the titanium content is varied.

The X-ray analyses of freshly prepared and used catalyst samples were compared. The comparison showed no change in the phase composition.

Raman Spectroscopy

Figure 2 displays the Raman spectra recorded for a selection of Sb–V–Ti–O catalysts being used in propane ammoxidation. The catalyst samples with vanadium are poor Raman scatterers and the spectra show only peaks with low intensities. A predominant spectral feature is a broad band at about 880 cm^{-1}, which irrespective of the titanium content is present in the spectra of all the catalysts containing vanadium. The intensity of the band, moreover, increases with the titanium content of the sample up to $x = 0.7$ in nominal $Sb_{0.9}V_{0.9-x}Ti_xO_y$. Compared with SVT-927, the intensity of the band was lower for SVT-918 (not shown in the figure) and Fig. 2 shows that the band is not present in the spectrum of SVT-909. Comparison of the spectra with the spectrum for α-Sb_2O_4 shows that the amount of α-Sb_2O_4 generally increases as the amount of titanium in the sample is increased. The strongest peaks from α-Sb_2O_4 are at 201, 400, and 464 cm^{-1} (5, 23). It is also evident that there is no TiO_2 of the rutile phase in the samples, since the two most prominent peaks at 610 and 447 cm^{-1} (24) are not visible. Bands from the anatase phase of TiO_2 at 638, 516, and 395 cm^{-1} (24) are clearly visible in the spectrum of SVT-909 and these bands were also present in the spectrum of SVT-918. In the spectrum of SVT-927 there is a weak feature around 638 cm^{-1}, which may be from anatase. Moreover, there is no V_2O_5 present in the samples as the typical strong peaks of V_2O_5 at 285, 700, and 995 cm^{-1} (6) are absent.

No significant change in the phase composition was observed comparing the Raman spectra of freshly prepared

TABLE 2

Unit Cell Parameters of the Rutile-Type Phase in Prepared Sb–V–Ti–O Catalysts

Catalyst notation	a (Å)	c (Å)	c/a
SVT-990	4.62(8)	3.03(5)	0.656
SVT-981	4.62(9)	3.03(2)	0.655
SVT-972	4.63(2)	3.00(2)	0.648
SVT-963	4.62(8)	3.03(5)	0.656
SVT-954	4.62(9)	3.02(4)	0.653
SVT-945	4.62(5)	3.00(6)	0.650
SVT-936	4.63(2)	3.02(3)	0.653
SVT-927	4.63(7)	3.00(5)	0.648
SVT-918	—[a]	—[a]	—[a]

[a] Could not be determined because too few rutile lines were visible.

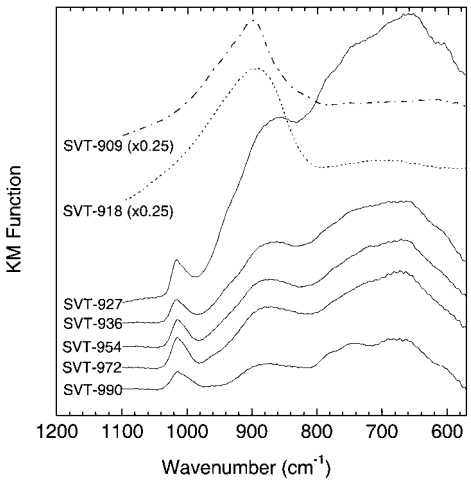

FIG. 3. DRIFT spectra of some freshly prepared Sb–V–Ti–O catalysts.

samples with the corresponding spectra of the samples being used in propane ammoxidation. As an example the spectra for the used and the freshly prepared SVT-963 are both given in Fig. 2.

Diffuse Reflectance FTIR Spectroscopy

Infrared bands in the region below 1200 cm^{-1} provide information about the metal–oxygen vibrations in metal oxides. DRIFT spectra from this region of some freshly prepared samples are presented in Fig. 3. Except for the spectra of the SVT-918 and SVT-909 samples with high titanium contents, the other catalyst spectra are characterized by a peak at 1015 cm^{-1} and broad bands at about 875 and 670 cm^{-1}. The intensities of the latter two bands increase with the titanium content. The bands at 1015 and 875 cm^{-1} are typical for the ≈$SbVO_4$ structure with Sb^{5+}, V^{4+}, and V^{3+} (18), and the band at 670 cm^{-1} is typical of rutiles (25, 26). These three bands disappear as the titanium content in the sample is increased above $x = 0.7$. For the sample without any vanadium (SVT-909), the spectrum in Fig. 3 shows only one band, which is intense and positioned at 900 cm^{-1}. The same band is present in the spectrum of SVT-918.

A comparison of DRIFT spectra recorded before and after use of SVT-918 and SVT-909 in propane ammoxidation did not show any change in the spectral features. The same observation was made for the other samples with the exception that the intensity of the band at 1015 cm^{-1} was decreased by about 10%.

Transmission Electron Microscopy and X-Ray Microanalysis

The SVT-963 preparation was investigated using transmission electron microscopy and energy dispersive X-ray analysis. The sample showed a fairly large variability in particle size and composition, ranging from pure antimony oxide to varying compositions of Sb, V, and Ti. However, the majority of the material was in the form of agglomerated particles in the size range 20–30 nm (Fig. 4). High-magnification images of the particles (Fig. 5) showed that the particles were crystalline with facets and smoothly rounded corners. The electron diffraction pattern is shown in Fig. 6a. The innermost ring is slightly diffuse due to Scherrer broadening of scattering from smaller particles, but the presence of more isolated reflections, best visible at higher frequencies (lower *d*-spacings), verifies an average crystallite size of 20–30 nm. The innermost ring of the electron diffractogram was calibrated toward the first line of the X-ray diffractogram of the same sample, and a good correlation with literature data of $SbVO_4$ (27) is found as shown in Table 3. The lattice spacing measured in images repeatedly (3.25 ± 0.1 Å) is consistent with the d_{110} spacing of the rutile-type structure. XEDS analysis of the group of particles in Fig. 4 showed no titanium in the crystals. However, electron diffraction patterns of other groups of particles with $Sb : V : Ti = 9 : 6 : 3$, corresponding to the nominal composition of the sample, showed great similarity (Fig. 6b, Table 3), supporting the concept that an exchange of V for Ti can be achieved without destroying the basic rutile-type structure.

The XEDS analyses of 15 different particles of SVT-963 have been collected in Fig. 7, showing that their compositions differ. A few particles are rich in titanium, while others are almost without titanium. However, most particles (Nos. 6–11 in Fig. 7) show a composition close to the nominal value for SVT-963, which is 50, 33, and 17 at.% of Sb, V, and Ti, respectively.

Activity Measurements

Activity measurements concerning the ammoxidation of propane were conducted on the samples listed in Table 1. Only the samples with vanadium were active. SVT-909 without vanadium was inactive. The initial reaction rates and

TABLE 3

Electron Diffraction Powder Rings from SVT-963 as Measured from Figs. 6a and 6b, Corresponding Real Space *d*-Values, and Literature Data

	d (Å)		$SbVO_4$[a]		
Ring	Fig. 6a	Fig. 6b	d_{hkl} (Å)	I/I_0	*hkl*
1	3.25	3.25	3.25	100	110
2	2.53	2.50	2.555	60	101
3	2.24	2.22	2.233	10	111
4	2.07	Too weak	2.055	4	210
5	1.71	1.68	1.71	50	211
6	1.64	Too weak	1.62	18	220
7	1.52	Too weak	1.539	6	002
8	1.47	Too weak	1.454	10	310
9	1.38	1.34	1.372	14	112

[a] Data from Ref. (27).

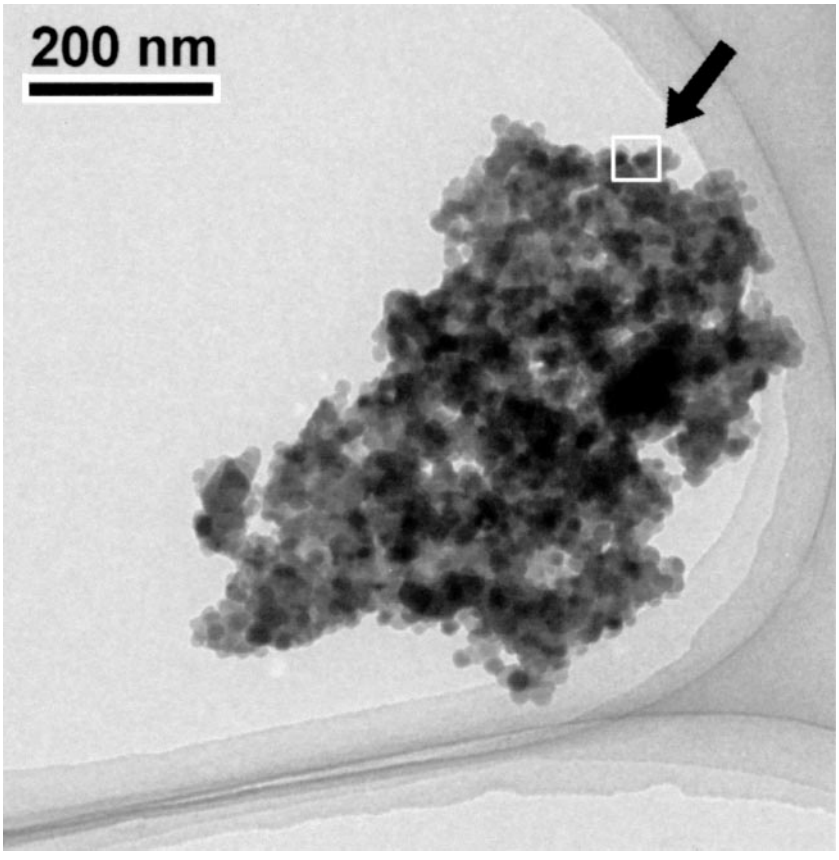

FIG. 4. TEM micrograph of SVT-963 showing an agglomeration of small particles, 20–30 nm in diameter, on a holey carbon grid. The marked area is enlarged in Fig. 5.

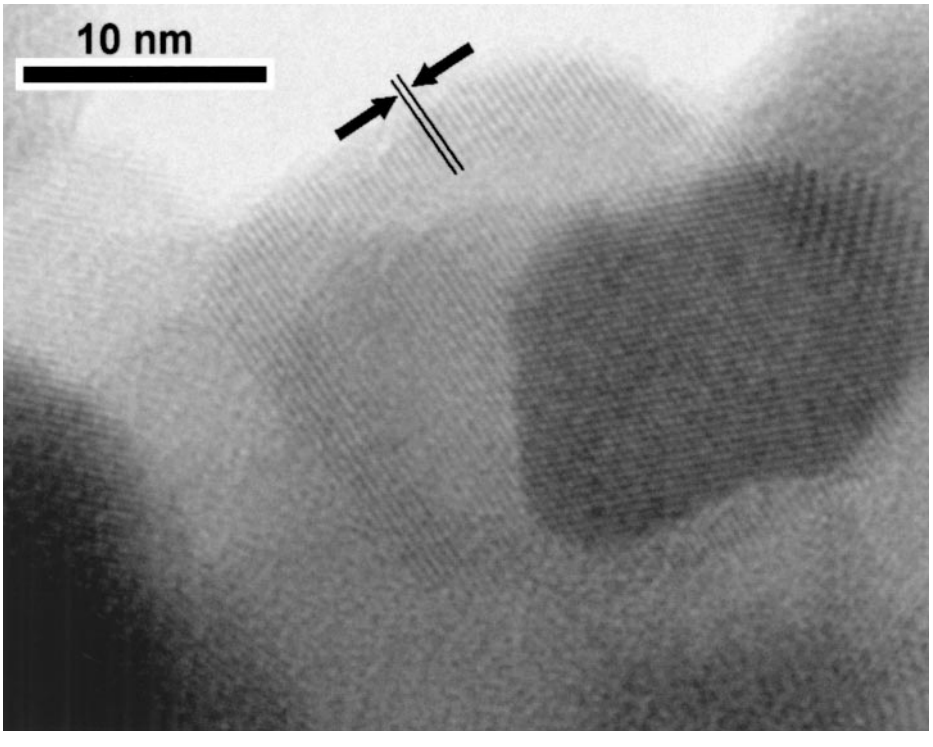

FIG. 5. High-resolution TEM image of the crystalline particles in Fig. 4. The indicated spacing corresponds to 3.25 Å. Moire fringes from overlapping crystals can be seen in some areas.

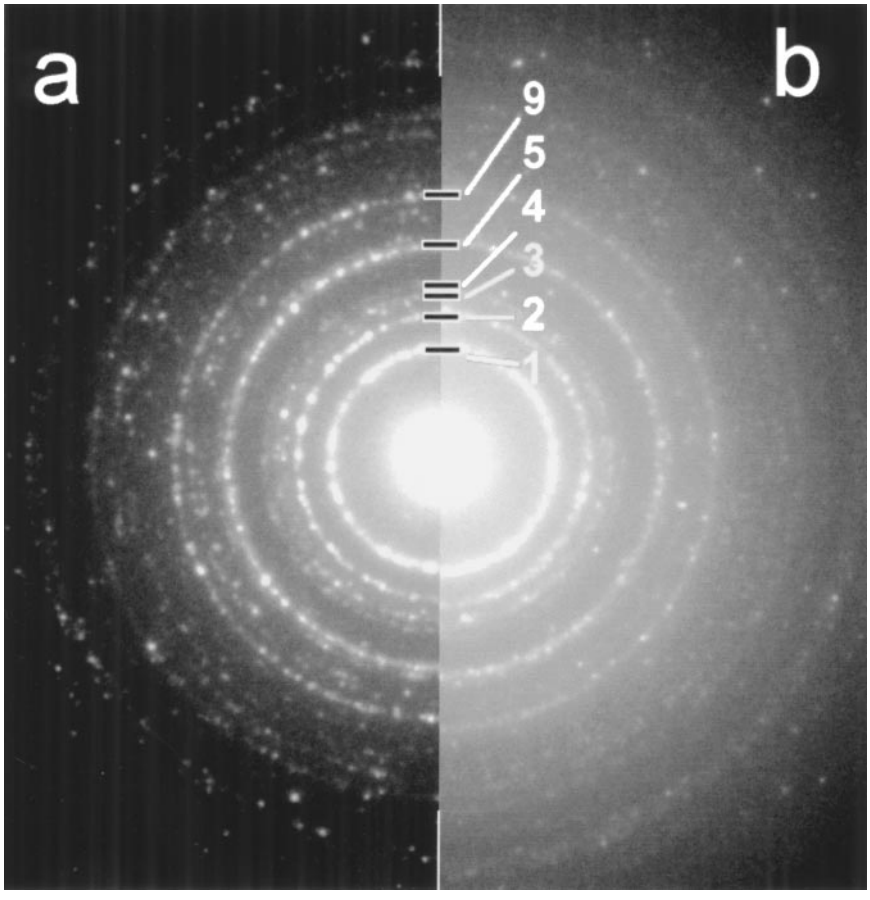

FIG. 6. Selected area diffraction patterns from (a) an area with no Ti present, shown in Fig. 4, and (b) an area with similarly sized particles but with a chemical composition of Sb : V : Ti = 9 : 6 : 3, corresponding to the nominal composition of the preparation. Numbers correspond to rings in Table 3.

the selectivities to the C_3 products propylene and acrylonitrile at 5, 15, and 25% propane conversion are displayed in Fig. 8. The levels of conversion were chosen to represent the initial product distribution and to show the ability of the catalysts to convert the propylene formed to acrylonitrile. The latter point is of great importance since it has been shown that the major intermediate in acrylonitrile formation from propane is propylene (4, 6, 8, 22).

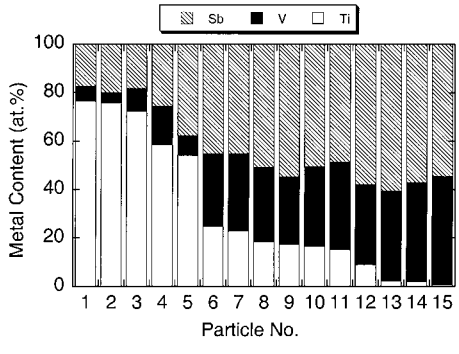

FIG. 7. X-ray microanalyses (XEDS) of 15 different particles in SVT-963.

The data in Fig. 8 show the trend that the activity of the catalyst decreases as the vanadium content is decreased. Moreover, regarding the catalytic performance the catalysts can be divided into three compositional regions corresponding to low, intermediate, and high titanium content. SVT-990, i.e., the pure ≈$SbVO_4$, is active to propylene formation at low propane conversion. With an increase in the propane conversion from 5 to 25%, the selectivity to propylene decreases from about 55 to 15%. There is no corresponding increase in the selectivity to acrylonitrile formation, which passes through a maximum of about 12% at 15% propane conversion. The SVT-981 and SVT-972 samples show catalytic behavior similar to that of SVT-990.

Another group of catalysts comprises SVT-963, SVT-954, and SVT-945. These catalysts show different behavior than the catalysts with lower titanium content. At 5% propane conversion, the selectivity to propylene is about 60% and the selectivity to acrylonitrile is about 15%. As the conversion of propane is increased to 25%, the selectivity to propylene decreases to approximately 10% and in parallel the selectivity to acrylonitrile increases to 38–45%. Obviously,

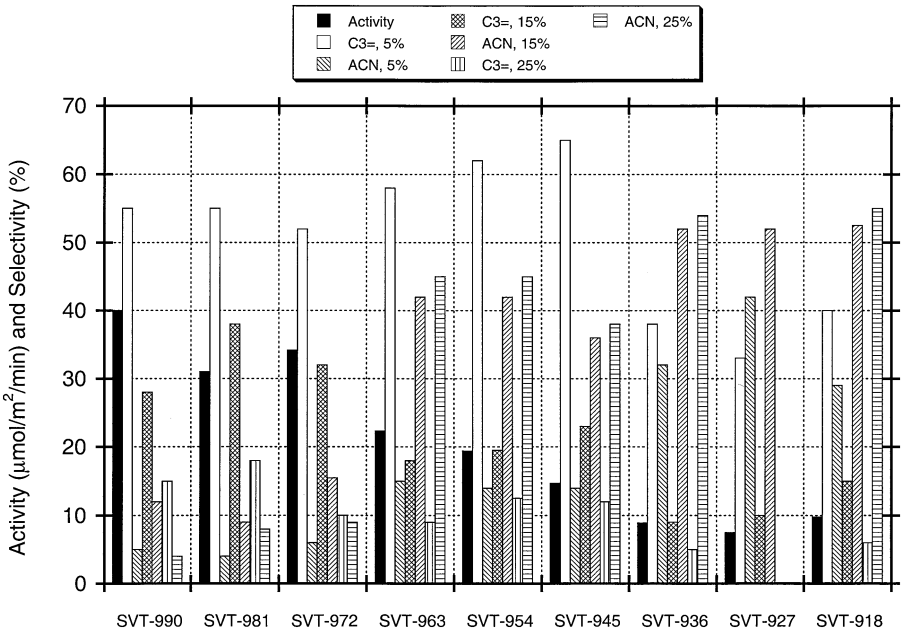

FIG. 8. Propane ammoxidation over Sb–V–Ti–O catalysts with varying V : Ti ratios. Initial reaction rates per surface area unit of catalyst (activity) and selectivities for propylene (C3=) and acrylonitrile (ACN) formations at 5, 15, and 25% of propane conversion. Reaction conditions: 480°C, 70 ml STP/min total flow with propane : ammonia : oxygen : steam : nitrogen = 1 : 1 : 2 : 0.5 : 2.5, and 100–3600 mg of catalyst.

this group of catalysts is able to convert the propylene formed to give acrylonitrile.

A third group of catalysts consists of SVT-936, SVT-927, and SVT-918. These catalysts, in addition to showing selectivity to propylene formation (≈35–40%) at 5% propane conversion, simultaneously produce acrylonitrile with a selectivity of about 30–40%. With an increase in the conversion of propane to 25%, the selectivity to propylene decreases to 5% (no data for SVT-927) and concurrently the selectivity to acrylonitrile formation reaches almost 55%.

The catalytic performances of three representative catalysts, one from each compositional region, are shown in Figs. 9–11. In addition to the selectivities to propylene and acrylonitrile, the selectivities to acetonitrile, hydrogen cyanide, carbon monoxide, and carbon dioxide have been plotted against the conversion of propane. Moreover, ethylene was formed with a selectivity that usually was below 1% and for high titanium contents it was up to 4% at low propane conversion. In addition to the information included in Fig. 8, the data for SVT-990 in Fig. 9 show that the selectivities to the nitrile products acrylonitrile, acetonitrile, and HCN all pass through a maximum when the conversion of propane is increased. It is worth noticing that the selectivity toward acetonitrile exceeds that for acrylonitrile. With an increase in the conversion of propane, the selectivities to propylene and the nitriles decrease due to combustion to carbon oxides, producing more carbon monoxide than carbon dioxide.

The catalytic data for SVT-963 in Fig. 10 show a considerable improvement of the catalytic properties compared with the data in Fig. 9 for SVT-990. In the same range of propane conversion (up to 25%) SVT-963 produces more acrylonitrile and gives less carbon oxides. The selectivity to acrylonitrile levels off below 50%, and the selectivity to acetonitrile does not exceed 8%. It can be observed that the

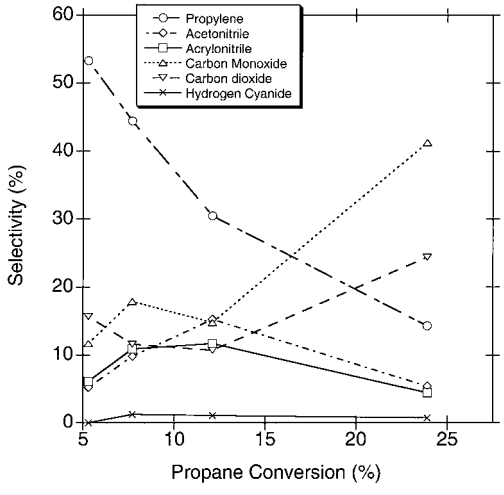

FIG. 9. Selectivity to propylene, acetonitrile, acrylonitrile, carbon oxides, and hydrogen cyanide as a function of the conversion of propane over SVT-990. Reaction conditions: 480°C, 70 ml STP/min total flow with propane : ammonia : oxygen : steam : nitrogen = 1 : 1 : 2 : 0.5 : 2.5, and 100–2400 mg of catalyst.

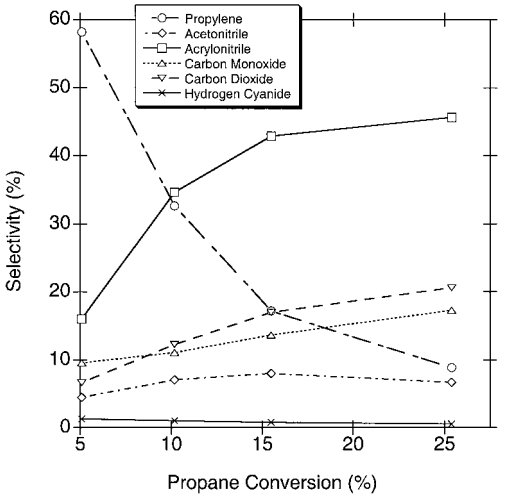

FIG. 10. Selectivity to propylene, acetonitrile, acrylonitrile, carbon oxides, and hydrogen cyanide as a function of the conversion of propane over SVT-963. Reaction conditions: 480°C, 70 ml STP/min total flow with propane : ammonia : oxygen : steam : nitrogen = 1 : 1 : 2 : 0.5 : 2.5, and 100–2400 mg of catalyst.

selectivity to the formation of carbon dioxide is somewhat higher than that to carbon monoxide.

According to the data in Fig. 8, SVT-936 is one of the best catalysts for acrylonitrile formation. Catalytic data for this catalyst, therefore, were collected up to 55% of propane conversion and are displayed in Fig. 11. The selectivity to propylene formation is high at low propane conversion and decreases steeply when the conversion of propane is increased. The selectivity to acrylonitrile reaches a maximum of 53% at about 25% propane conversion. When the conversion of propane is increased, the selectivity to acrylonitrile decreases and in parallel the selectivies to the carbon oxides increase. The selectivities to the formations of acetonitrile and HCN pass through maxima and do not exceed 8 and 2%, respectively.

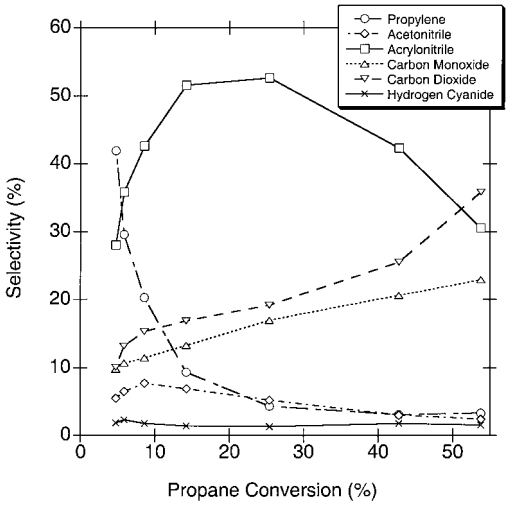

FIG. 11. Selectivity to propylene, acetonitrile, acrylonitrile, carbon oxides, and hydrogen cyanide as a function of the conversion of propane over SVT-936. Reaction conditions: 480°C, 70 ml STP/min total flow with propane : ammonia : oxygen : steam : nitrogen = 1 : 1 : 2 : 0.5 : 2.5, and 100–8400 mg of catalyst.

DISCUSSION

Substitution in ≈$SbVO_4$

For the Sb–V–Ti–O preparations with vanadium the XRD patterns in Fig. 1 show formation of a rutile-type phase. No split of the rutile reflections is observed, which indicates that only one rutile phase is present. The diffraction lines and the unit cell parameters in Table 2 for SVT-990 agree with the data being published for $Sb_{0.92}V_{0.92}\square_{0.16}O_4$ with cation vacancies (□) (17, 18) and also agree with the data being reported for $Sb_{1-x}V_{1-x}O_4$ (15, 16). Obviously, the two phases are identical. With an increase in the titanium content in the samples with vanadium, in addition to a rutile phase, there is an increase of the amount of α-Sb_2O_4 being formed (Fig. 1). Calculations using the XRD data obtained by powder diffraction show that the unit cell of the rutile phase in the samples with titanium does not differ much from that being determined for SVT-990; see Table 2. The electron diffraction ring patterns (Fig. 6 and Table 3), which are from a few hundred 20- to 30-nm particles, give of course less accuracy than powder XRD, which is the average of several million particles. However, the lateral resolution of the XEDS analysis is on the same order as or smaller than the area used for selected area diffraction. The SVT-963 sample (Fig. 6 and Table 3) shows lattice constants within the experimental error similar to those of the rutile-structure phase ≈$SbVO_4$, even though a large variability in the chemical composition can be demonstrated by XEDS (Fig. 7). It should be noticed that the ionic radii of Ti^{4+} (0.61 Å), V^{4+} (0.58 Å), V^{3+} (0.64 Å), and Sb^{5+} (0.60 Å) do not differ much (20) and, therefore, a great difference in the cell constants would not be expected.

The characterization of the preparations with FT-Raman spectroscopy (Fig. 2) clearly shows that there is no pure TiO_2 in the form of rutile present in the catalysts. This result supports the XRD data showing that there is only one type of rutile phase in the samples. Moreover, the presence of TiO_2 (anatase) in a significant amount is limited to the samples with high titanium contents (SVT-918, SVT-909) as shown by the XRD and Raman results. Neither Raman nor XRD shows formation of any free vanadium oxide. Thus, the results described prove that a rutile-type phase is formed in parallel with free α-Sb_2O_4 and, furthermore, that titanium substitution in ≈$SbVO_4$ occurs. The Raman band for SVT-990 at 880 cm^{-1} (Fig. 2) is typical of the cation-deficient ≈$SbVO_4$ structure (6, 8). The spectra in Fig. 2 reveal that the related ≈$SbVO_4$ with Ti in the structure gives the same Raman band.

The DRIFT spectra in Fig. 3 confirm the formation of a ≈$SbVO_4$-related rutile phase. The bands at 1015 and 875 cm^{-1} have been assigned to the ≈$SbVO_4$ structure with cation vacancies (6, 18) and are not bands from free V_2O_5. Crystalline V_2O_5 should give two infrared bands at 1020 and 820 cm^{-1} from metal–oxygen stretching modes involving one-coordinated and two-coordinated lattice oxygens, respectively (28). The infrared bands from the ≈$SbVO_4$-related phase are at slightly different positions and there are no strong bands from V_2O_5 at 995 and 700 cm^{-1} (6) in the corresponding Raman spectra in Fig. 2. Moreover, the characterization of the samples with electron microscopy, XEDS analysis, and XRD (Fig. 1) did not give evidence of any trace of V_2O_5 being present in the samples.

In a previous investigation formation of β-Sb_2O_4 with about 5% V in the lattice was observed on heating α-Sb_2O_4 and V_2O_5 (Sb : V = 20 : 1) at 810°C for 12 h (29). There is also a report that the same material can form at a lower temperature under influence from the ammoxidation of propylene (13). In the present work no indication of β-Sb_2O_4 formation was obtained. This may be due to the fact that the catalyst samples were calcined at 810°C for 1 h only and the activity of the material is considerably smaller for propane ammoxidation than for the same reaction with propylene (8).

Substitution Mechanism

The XEDS data in Fig. 7 for SVT-963 are plotted in a Sb–V–Ti composition triangle in Fig. 12. Two composition lines, A–B and A–Ti, in the figure have been drawn to describe the two simplest substitution mechanisms, which are

$$Ti^{4+} \leftrightarrow V^{4+} \quad [1]$$

$$2Ti^{4+} \leftrightarrow V^{3+} + Sb^{5+}. \quad [2]$$

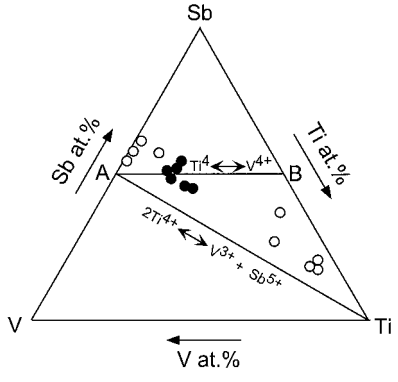

FIG. 12. Triangle plot of energy dispersive X-ray microanalyses of SVT-963. The Sb, V, and Ti contents (○, ●) of the 15 analyses in Fig. 7 have been plotted together with the two simplest substitution mechanisms for Ti in ≈$SbVO_4$, which are described by the composition lines A–B and A–Ti, respectively. The data points marked by the filled circles (●) represent compositions that are close to the nominal composition of the sample, i.e., 50 at.% Sb, 33 at.% V, and 17 at.% Ti.

It is evident from Fig. 12 that most crystals have a composition that is close to the nominal composition of the sample (50 at.% Sb, 33 at.% V, and 17 at.% Ti), which corresponds to mechanism [1] above. However, other crystals have compositions that are within the triangle A–B–Ti, being limited by the two lines describing the two substitution mechanisms. In these crystals, the substitution of titanium has evidently occurred according to both mechanisms, which agrees with the formation of some crystalline α-Sb_2O_4 in the samples (Figs. 1 and 2). Despite a slight overestimation of the Sb content, some crystals are poor in titanium and have compositions close to $Sb_{0.92}V_{0.92}O_4$. Thus, according to the data in Fig. 12 both substitution mechanisms occur, and a solid solution series with Ti in the $Sb^{5+}_{0.92}V^{3+}_{0.28}V^{4+}_{0.64}\square_{0.16}O_4$ phase (17) can be formulated as $Sb^{5+}_{(0.92-z/2)}V^{3+}_{(0.28-z/2)}V^{4+}_{(0.64-u)}Ti^{4+}_{(z+u)}\square_{0.16}O_4$, where □ is a cation vacancy. The upper limits for z and u were not determined, but it is obvious that all vanadium in ≈$SbVO_4$ cannot be replaced by titanium since the XRD pattern of SVT-909 did not show the formation of a rutile-type structure. A model will be described below and the results in Table 4 from this model indicate that the upper substitution limits are $z/2 \approx 0.28$ and $u \approx 0.40$. The occurrence of both substitution mechanisms agrees with the previous observation that V_2O_5 is formed in preparations with the nominal composition $VSb_{1-x}Ti_xO_4$ and, in addition to a rutile-related phase, α-Sb_2O_4 is formed, calcining samples of the nominal composition $V_{1-x}Ti_xSbO_4$ (30).

Considering the FT-Raman and DRIFT spectral features in Figs. 2 and 3 it becomes clear that the cation vacancies are retained in the solid solution being formed. A linear relationship between the number of cation vacancies and the intensities of the two infrared bands at 1015 and 875 cm^{-1} have been reported for $Sb_{0.9}V_{0.9+x}\square_{0.2-x}O_4$ (18). Also, the Raman band at about 880 cm^{-1} is characteristic of ≈$SbVO_4$ with cation vacancies (6, 8). The intensities of these IR and Raman bands have been demonstrated to decrease upon reduction of the material and completely disappear when $Sb_{0.9}V_{0.9+x}\square_{0.2-x}O_4$ is reduced, forming $Sb_{0.9}V_{1.1}O_4$ (6, 8, 18), which is a stoichiometric rutile-type structure without cation vacancies (18). The latter composition corresponds to those that, in the past, have been described as $Sb_{1-y}V_{1+y}O_4$ (15), $Sb_{1-y}VO_{4-1.5y}$, and $Sb_{1-y}VO_{4-2y}$ (16). The infrared bands at 1015 and 875 cm^{-1} are not typical of the rutile structure. In rutiles all oxygens are three-coordinated and the metal–oxygen vibrations appear in four principal regions, which are around 730–630, 580–500, 375–250, and 190–160 cm^{-1} (25). In the cation-deficient ≈$SbVO_4$ rutile structure, some lattice oxygens are two-coordinated (17). Thus, the infrared bands at 1015 and 875 cm^{-1} can be assigned to metal–oxygen vibrations involving the two-coordinated oxygen species, which are located at cation vacancies. Considering the distortion requirements on the rutile structure to

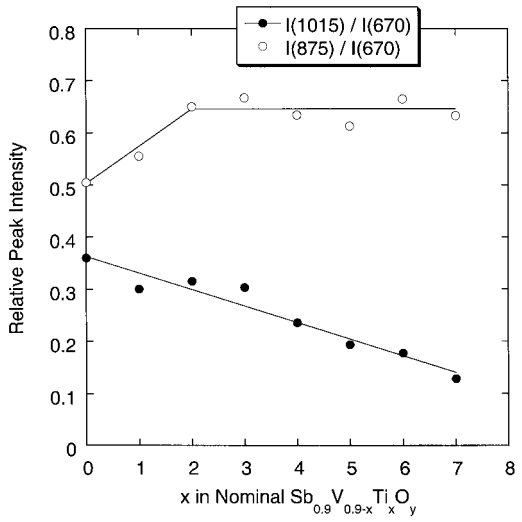

FIG. 13. The intensities of the DRIFT bands at 1015 and 875 cm^{-1} relative to that at 670 cm^{-1} plotted versus x in nominal $Sb_{0.9}V_{0.9-x}Ti_xO_y$. For estimating the relative intensities of the peaks, a linear and horizontal baseline was drawn from 1050 cm^{-1}.

accommodate a two-coordinated oxygen species, it was demonstrated that the two-coordinated oxygens are in the following configurations ordered in sequence of probability $OSb_2\square > OSbV\square > OV_2\square$ (17). The infrared band at 1015 cm^{-1} is a typical vanadyl band (31) and can be assigned to a $V^{4+}{=}O$ vibration of the second most favorable configuration, and the band at 875 cm^{-1} can be from a Sb–O–Sb stretching mode of the most favorable configuration (6).

With an increase of the titanium content of the catalyst the intensity of the DRIFT band at 1015 cm^{-1} decreases relative to that of the typical rutile band at 670 cm^{-1} (Fig. 3). The intensity ratio has been plotted in Fig. 13, which shows an almost linear decrease of the ratio with an increase in the x-value of the nominal $Sb_{0.9}V_{0.9-x}Ti_xO_y$ preparations. This relationship can be seen as a consequence of V^{4+} in the cation-deficient rutile structure being replaced by Ti^{4+}. In Fig. 13 is also plotted the relative intensity of the band at 875 cm^{-1}, the relative intensity of which first increases with an increase in the x-value and then levels off. This relationship is due to the replacement of V^{4+} with Ti^{4+} in the $OSbV\square$ position forming $OSbTi\square$ and the same moiety can form when a V^{3+}/Sb^{5+} pair is replaced with two Ti^{4+}. Both the DRIFT and the FT-Raman spectra in Figs. 2 and 3 in most cases show a band at around 880 cm^{-1}, which in both cases possibly originates from the same species. The intensity of the Raman band increases with the titanium content of the sample (Fig. 2), while the infrared band does not show the same pronounced increase (Figs. 3 and 13). This can be due to the fact that in infrared, the band is positioned on top of a broad band, which makes it difficult to draw a correct baseline for quantitative comparison. The increase of the intensity of the Raman band with an increase of the Ti content therefore better reflects the substitution of titanium. However, the scattering property of the sample may also be affected by the substitution of titanium.

Composition of the Rutile Phase in the Sb–V–Ti–O Catalysts

It was observed that $Sb_{0.9}V_{0.9}O_4$ with the vanadium predominantly in the 4+ state gives an infrared band at 1015 cm^{-1}, while this band is not present in the infrared spectrum of $Sb_{0.9}V_{1.1}O_4$ with the vanadium essentially in the 3+ state (18). Therefore, assuming that the DRIFT band at 1015 cm^{-1} is a measure of the number of V^{4+} ions in the unit cell and starting from the substitution formula $Sb^{5+}_{(0.92-z/2)}V^{3+}_{(0.28-z/2)}V^{4+}_{(0.64-u)}Ti^{4+}_{(z+u)}\square_{0.16}O_4$ (17), the coefficient $(0.64-u)$ can be determined from the data points in Fig. 13, calculating the intensity ratio of the band at 1015 cm^{-1} to the same band in the pure $Sb_{0.92}V_{0.92}O_4$ (SVT-990). Since no free vanadium oxide is formed in the syntheses and no free TiO_2 is present in a broad range of composition, having determined the u-value in the formula, the z-value can be calculated from the nominal V : Ti ratio of the sample. Finally, the amount of Sb in the form of free α-Sb_2O_4 is easily obtained. The data obtained from the model calculations are presented in Table 4. Although the TEM/XEDS results show that the composition of the rutile phase varies between the crystals in each sample (Fig. 7), the DRIFT spectra are representative of the bulk of the material and the use of the band at 1015 cm^{-1} for quantitative purpose should reflect the average composition of the material.

The data in Table 4 explain the formation of α-Sb_2O_4. To verify the results as being reasonable, the calculated amount of Sb present as α-Sb_2O_4 relative to the total number of cations in the sample is plotted in Fig. 14 against the ratio $d_{112}/(d_{110}+d_{112})$, which is obtained from the XRD pattern and where d_{112} and d_{110} are the strongest reflections from α-Sb_2O_4 (JCPDS-file 11-694) and ≈$SbVO_4$ (JCPDS-file 16-600), respectively (32). It is seen that a linear relationship exists, which gives some support for the calculated compositions being reasonable. The intercept of the graph with the x-axis is about 6%, which is fairly good, since the lower detection limit using X-ray diffraction usually is about 5%. Attempts were made to determine calibration factors for α-Sb_2O_4 and the rutile phase. However, these attempts failed because the absolute intensity of the rutile peaks varied with the degree of substitution with titanium and pure reference compounds were not available.

Considering the calculated compositions in Table 4 it is worthy of notice that the catalysts can broadly be divided into three compositional groups as indicated in Table 5. Thus, the catalytic data in Fig. 8 can be understood since not only the composition of the catalysts in each group is similar but so is the catalytic behavior.

TABLE 4

Composition of Rutile-Type $\approx(Sb,V,Ti)_{1.8}O_4$ in Prepared Catalysts and the Relative Amount of Sb Present in the Form of Free α-Sb_2O_4 as Calculated from the Relative Intensity of the DRIFT Band at 1015 cm^{-1} and the V : Ti Atomic Ratio of the Sample

Catalyst	Composition of rutile-type $Sb^{5+}_{(0.92-z/2)}V^{3+}_{(0.28-z/2)}V^{4+}_{(0.64-u)}Ti^{4+}_{(z+u)}\square_{0.16}O_4$, ($\square$ = cation vacancy)				Number of Sb atoms in the form of free Sb_2O_4/(Sb + V + Ti) atoms in total (%)
	$(0.92-z/2)Sb^{5+}$	$(0.28-z/2)V^{3+}$	$(0.64-u)V^{4+}$	$(z+u)Ti^{4+}$	
SVT-990	0.92	0.28	0.64	0	0
SVT-981	0.92	0.28	0.53	0.11	0
SVT-972	0.85	0.21	0.56	0.22	7.1
SVT-963	0.80	0.16	0.54	0.35	11.8
SVT-954	0.80	0.16	0.42	0.46	10.9
SVT-945	0.77	0.13	0.34	0.59	13.8
SVT-936	0.70	0.06	0.31	0.76	19.0
SVT-927	0.67	0.03	0.23	0.91	21.2
SVT-918	—[a]	—[a]	—[a]	—[a]	—[a]

[a] Could not be determined since no DRIFT peak was visible at 1015 cm^{-1} (see Fig. 3).

Structure–Reactivity Relationships

One of the aims of the investigation was to substitute Ti for V and thereby determine the roles of the elements and their oxidation state. Due to the two substitution mechanisms described occurring in parallel, both V^{4+} and a V^{3+}/Sb^{5+} pair are replaced by Ti^{4+}. This fact complicates the search for structure–reactivity correlations, and data from several techniques must be combined for quantitative treatment causing some reasonable scattering of the data.

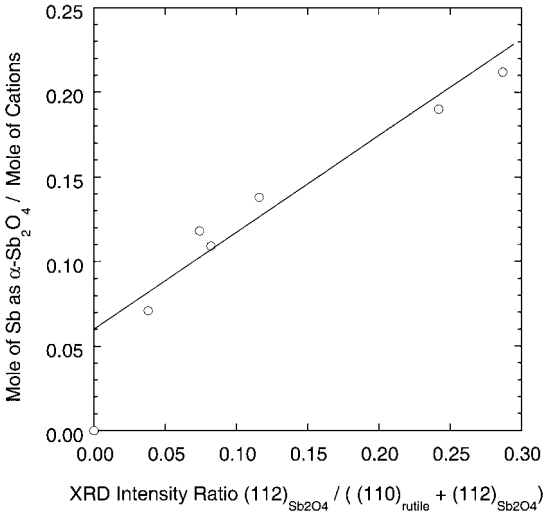

FIG. 14. Moles of Sb present in the sample in the form of α-Sb_2O_4 relative to the total number of moles of Sb, V, and Ti in the sample plotted versus the intensity ratio of the (112) reflection from α-Sb_2O_4 relative to the sum of the intensity of the (110) reflection from $\approx(Sb,V,Ti)_2O_4$ and the (112) reflection from α-Sb_2O_4. The calculation of the number of moles of Sb in the sample is described in the text.

We have tried to correlate activity and selectivity to the various elements and their oxidation state in the catalysts. The best fits were obtained correlating the activity to the V^{3+} content of the unit cell of the rutile-type phase, and a reasonable correlation of the selectivity to acrylonitrile with the $Sb^{5+} : V^{3+}$ ratio of the unit cell was observed. The relationships are shown in Figs. 15 and 16. For the correlation of activity it is reasonable to neglect the contribution from α-Sb_2O_4 to the specific surface area of the catalyst, since the α-Sb_2O_4 crystals in this type of material are usually much larger than the rutile crystals (5, 12) and then have a low level of activity (6–8). A relationship between the activity and the V^{3+} content (Fig. 15) is reasonable because the hydrogen abstraction from propane is rate-limiting (6, 33–35) and it is generally believed that elements with a lone pair

TABLE 5

Ranking of the Prepared Sb–V–Ti–O Catalysts into Three Compositional Groups Based on the Data in Table 4

Group	Catalyst	Atom content of the $(Sb,V,Ti)_{1.8}\square_{0.2}O_4$ unit cell ($\square$ = cation vacancy)			
		Sb^{5+}	V^{3+}	V^{4+}	Ti^{4+}
I	SVT-990, SVT-981, SVT-972	≈0.9	≈0.25	≈0.6	0–0.2
II	SVT-963, SVT-954, SVT-945	≈0.8	≈0.15	0.3–0.5	0.3–0.6
III	SVT-936, SVT-927, SVT-918[a]	≈0.7	<0.1	0.2–0.3	0.7–0.9

Note. According to the selectivity data in Fig. 8, each group shows characteristic behavior.

[a] Could not be determined since no DRIFT peak was visible at 1015 cm^{-1} (see Fig. 3).

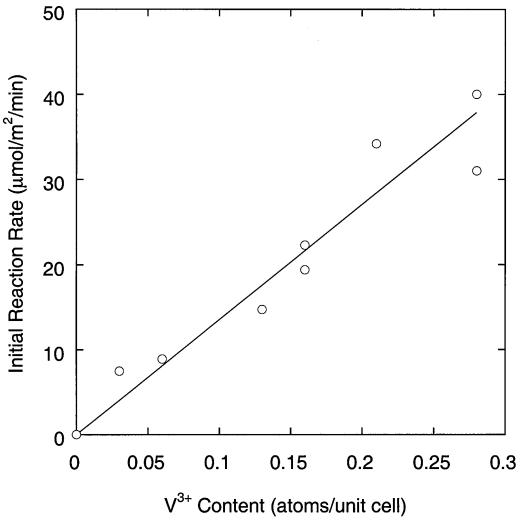

FIG. 15. Initial reaction rate for the Sb–V–Ti–O preparations as a function of the V^{3+} content of the unit cell of the rutile as given in Table 4.

of electrons (filled valence *s*-orbital), e.g., Bi^{3+} in catalysts for propylene ammoxidation, are capable of performing the first abstraction of hydrogen (36, 37). The fact that V^{3+} has a filled 4*s* orbital imparts a partial radical character to the oxygen, i.e., V–O·, making possible the facile attack on the C–H bond in propane.

Great caution must be exercised in correlating the selectivity to acrylonitrile with the structural characteristics of the catalyst, since the nitrogen insertion step is not rate-determining. However, as Fig. 16 shows, there is a relationship between the selectivity to acrylonitrile formation and the $Sb^{5+}:V^{3+}$ ratio of the unit cell of the rutile phase. The selectivity to acrylonitrile at 5% propane conversion was

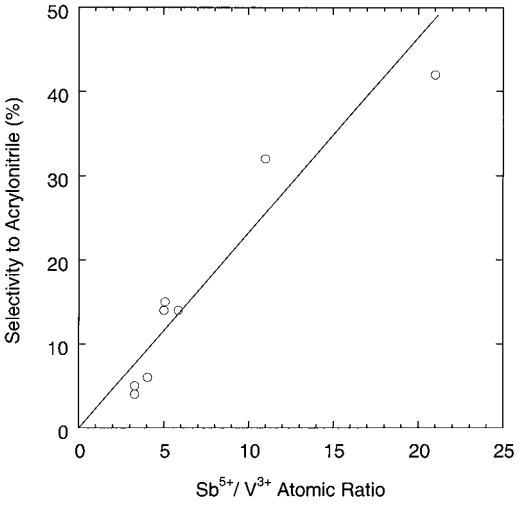

FIG. 16. Selectivity to the formation of acrylonitrile at 5% propane conversion versus the $Sb^{5+}:V^{3+}$ atomic ratio of the unit cell as calculated from the data in Table 4.

selected for the plot because low propane conversion minimizes the influence on the data from consecutive degradation pathways. The relationship observed suggests that Sb is the nitrogen-inserting component. This inference can be perceived considering that the V^{3+} species is the propane activator and if Sb^{5+} performs the nitrogen insertion, then an increase in the $Sb^{5+}:V^{3+}$ ratio of the active material should increase the probability of nitrogen insertion and formation of acrylonitrile. The conclusion that Sb^{5+} species are the NH_3 activation sites agrees with the finding that Sb^{5+} cations in the form of Sb^{5+}-NH-Sb^{5+} moities are responsible for the nitrogen insertion step in the ammoxidation of propylene over iron and uranium antimonate catalysts (38). In the latter catalysts, the coexistence of Sb^{3+}/Sb^{5+} pairs has been observed and a bridging oxygen species associated with the Sb^{3+} polyhedron performs the rate-limiting first abstraction of a hydrogen atom from propylene. In the $\approx(Sb,V,Ti)_{1.8}O_4$ catalysts, which are active and selective for propane ammoxidation, our results show the necessity of having V^{3+}/Sb^{5+} pairs. It is possible that the oxygen associated with V^{3+}, compared with an Sb^{3+} oxygen, is more suited to propane activation.

Most partial oxidation catalysts used commercially contain a redox component to maintain the activity of the catalyst by promoting rapid reoxidation and reconstruction of the active sites. For example, the redox couple in iron and uranium antimonate is Fe^{2+}/Fe^{3+} and U^{5+}/U^{6+}, respectively (36, 37). In $\approx(Sb, V, Ti)_{1.8}O_4$ catalysts this role may be assigned to vanadium and the $V^{4+}{=}O$ species responsible for the infrared band at 1015 cm^{-1} (see Fig. 3). As already mentioned, the band at 1015 cm^{-1} is typical of the oxidized form of $\approx SbVO_4$, i.e., the cation-deficient $Sb_{0.92}V_{0.92}O_4$ with predominantly V(IV) states. Upon reduction of the oxidized phase, the stoichiometric phase $Sb_{0.9}V_{1.1}O_4$ with predominantly V(III) states is formed together with some α-Sb_2O_4. As opposed to the oxidized form of the rutile, the reduced phase presents no infrared band at 1015 cm^{-1} (18). The reoxidation process is obviously facile in the Sb–V–Ti–O catalysts and not rate-limiting, since the intensity of the infrared band at 1015 cm^{-1} had not decreased much after the samples were used in propane ammoxidation. Moreover, the decrease was more or less independent of the titanium content of the catalyst.

The catalytic results in Figs. 8–11 and the relationship in Fig. 16, moreover, are consistent with the site isolation theory, according to which it is necessary to have structurally isolated sites with a suitable number of oxygen species of appropriate metal–oxygen bond strength to avoid waste formation and obtain a selective ammoxidation catalyst (10, 11). The data in Figs. 8 and 16 show that the substitution of titanium into the catalyst structure contributes to the vanadium site isolation and dispersion, hence making the catalyst much more selective to acrylonitrile formation. Creating isolation of the vanadium sites in the structure reduces

the number of V–O–V pairs, which possibly are degradation sites for propane and subsequently formed propylene, producing C_1 and C_2 products.

CONCLUSIONS

Compared with the pure cation-deficient $\approx SbVO_4$, Ti substitution in $\approx SbVO_4$ produces a lower level of activity but improved selectivity to acrylonitrile in the ammoxidation of propane. Characterization of preparations with the nominal composition $Sb_{0.9}V_{0.9-x}Ti_xO_y$ and with various titanium content evidences the formation of a rutile-type phase with Ti^{4+} replacing both V^{4+} and a V^{3+}/Sb^{5+} pair, forming the solid solution series $Sb^{5+}_{(0.92-z/2)}V^{3+}_{(0.28-z/2)}V^{4+}_{(0.64-u)}Ti^{4+}_{(z+u)}\square_{0.16}O_4$ with cation vacancies ($\square$).

A correlation exists between the activity and the V^{3+} content of the unit cell of the rutile phase. Likewise, there is a correlation between the selectivity to acrylonitrile and the $Sb^{5+}:V^{3+}$ ratio of the rutile phase. The relationships indicate that V^{3+} sites are engaged in the activation of propane and that the activation of ammonia involves Sb^{5+} centers.

ACKNOWLEDGMENTS

The Swedish Research Council for Engineering Sciences (TFR) and the Swedish Natural Science Research Council (NFR) are acknowledged for financial support. Mrs. Birgitta Svensson is acknowledged for making the BET and XRD measurements, and Miss Pernilla Nevsten is acknowledged for assisting in parts of the TEM/XEDS investigation.

REFERENCES

1. Grasselli, R. K., *in* "Handbook of Heterogeneous Catalysis" (G. Ertl, H. Knözinger, and J. Weitkamp, Eds.), p. 2302. Wiley–VCH, New York, 1997.
2. Grasselli, R. K., *Catal. Today* **49**, 141 (1999).
3. Guttmann, A. T., Grasselli, R. K., and Brazdil, J. F., U.S. Patent 4,746,641 (1988). [Assigned to the Standard Oil Company (OH)]
4. Centi, G., Grasselli, R. K., and Trifirò, F., *Catal. Today* **13**, 661 (1992).
5. Nilsson, J., Landa-Cánovas, A. R., Hansen, S., and Andersson, A., *J. Catal.* **186**, 442 (1999).
6. Nilsson, R., Lindblad, T., and Andersson, A., *J. Catal.* **148**, 501 (1994).
7. Nilsson, J., Landa-Cánovas, A. R., Hansen, S., and Andersson, A., *J. Catal.* **160**, 244 (1996).
8. Nilsson, R., Lindblad, T., Andersson, A., Song, C., and Hansen, S., *in* "New Developments in Selective Oxidation II" (V. Cortés Corberán and S. Vic Bellón, Eds.), Studies in Surface Science and Catalysis, Vol. 82, p. 293. Elsevier, Amsterdam, 1994.
9. Nilsson, J., Landa-Cánovas, A. R., Hansen, S., and Andersson, A., *in* "3rd World Congress on Oxidation Catalysis" (R. K. Grasselli, S. T. Oyama, A. M. Gaffney, and J. E. Lyons, Eds.), Studies in Surface Science and Catalysis, Vol. 110, p. 413. Elsevier, Amsterdam, 1997.
10. Callahan, J. L., and Grasselli, R. K., *AIChE J.* **9**, 755 (1963).
11. Grasselli, R. K., and Burrington, J. D., *in* "Advances in Catalysis" (D. D. Eley, H. Pines, and P. B. Weisz (Eds.), Vol. 30, p. 133. Academic Press, New York, 1981.
12. Nilsson, J., Landa-Cánovas, A. R., Hansen, S., and Andersson, A., *Catal. Today* **33**, 97 (1997).
13. Berry, F. J., and Brett, M. E., *J. Catal.* **88**, 232 (1984).
14. Nilsson, R., Lindblad, T., and Andersson, A., *Catal. Lett.* **29**, 409 (1994).
15. Birchall, T., and Sleight, A. W., *Inorg. Chem.* **15**, 868 (1976).
16. Berry, F. J., Brett, M. E., and Patterson, W. R., *J. Chem. Soc. Dalton Trans.*, 9 (1983).
17. Hansen, S., Ståhl, K., Nilsson, R., and Andersson, A., *J. Solid State Chem.* **102**, 340 (1993).
18. Landa-Cánovas, A., Nilsson, J., Hansen, S., Ståhl, K., and Andersson, A., *J. Solid State Chem.* **116**, 369 (1995).
19. Baur, W. H., *Z. Kristallogr.* **209**, 143 (1994).
20. Aylward, G., and Findlay, T., "SI Chemical Data," 4th ed. Wiley, Brisbane, 1998.
21. Lynch, C. S., Glaeser, L. C., Brazdil, J. F., and Toft, M. A., U.S. Patent 5,094,989 (1992). [Assigned to the Standard Oil Company (OH)]
22. Catani, R., Centi, G., Trifirò, F., and Grasselli, R. K., *Ind. Eng. Chem. Res.* **31**, 107 (1992).
23. Cody, C. A., DiCarlo, L., and Darlington, R. K., *Inorg. Chem.* **18**, 1572 (1979).
24. Deo, G., Turek, A. M., Wachs, I. E., Machej, T., Haber, J., Das, N., Eckert, H., and Hirt, A. M., *Appl. Catal. A* **91**, 27 (1992).
25. Rocchiccioli-Deltcheff, C., Dupuis, T., Franck, R., Harmelin, M., and Wadier, C., *C.R. Acad. Sci. Paris Ser. B* **270**, 541 (1970).
26. Husson, E., Repelin, Y., Brusset, H., and Cerez, A., *Spectrochim. Acta Sect. A* **35**, 1177 (1979).
27. Roth, R. S., and Waring, J. L., *Am. Miner.* **48**, 1348 (1963).
28. Abello, L., Husson, E., Repelin, Y., and Lucazeau, G., *Spectrochim. Acta Sect. A* **39**, 641 (1983).
29. Berry, F. J., Brett, M. E., and Patterson, W. R., *J. Chem. Soc. Dalton Trans.*, 13 (1983).
30. Berry, F. J., Smart, L. E., and Duhalde, S., *Polyhedron* **15**, 651 (1996).
31. Barraclough, C. G., Lewis, J., and Nyholm, R. S., *J. Chem. Soc.*, 3552 (1959).
32. JCPDS International Centre for Diffraction Data, "Powder Diffraction File," Swarthmore, PA, 1991.
33. Nilsson, R., and Andersson, A., *Ind. Eng. Chem. Res.* **36**, 5207 (1997).
34. Brazdil, L. C., Ebner, A. M., and Brazdil, J. F., *J. Catal.* **163**, 117 (1996).
35. Michaels, J. N., Stern, D. L., and Grasselli, R. K., *Catal. Lett.* **42**, 139 (1996).
36. Grasselli, R. K., *J. Chem. Educ.* **63**, 216 (1986).
37. Grasselli, R. K., Brazdil, J. F., and Burrington, J. D., *Appl. Catal.* **25**, 335 (1986).
38. Burrington, J. D., Kartisek, C. T., and Grasselli, R. K., *J. Catal.* **87**, 363 (1984).